Investigation of Riverbank Peat Erosion in a small Alpine catchment by Multi-Temporal Point Cloud Change Analysis and Time Series Clustering

Jiapan Wang[1*], Rasoul Eskandari[2*], ChengHan Lin[3*], János Mészáros[4*], Laura Obrecht[5*], Evangeline Rowe[6*], Jules Salzinger[7*], Martin Rutzinger[8], Andreas Mayr[8]

[1] TUM School of Engineering and Design, Technical University of Munich, Germany - jiapan.wang@tum.de
[2] Dept. of Architecture, Built Env. and Construction Engineering, Politecnico di Milano, Italy - rasoul.eskandari@polimi.it
[3] Dept. of Civil Engineering, National Yang Ming Chiao Tung University, Taiwan - chenghan.stephan.lin@proton.me
[4] HUN-REN Centre for Agricultural Research, Institute for Soil Sciences, Hungary - meszaros.janos@atk.hun-ren.hu
[5] Inst. of Geography and Geology, Physical Geography, Univ. of Würzburg, Germany - laura.obrecht@stud-mail.uni-wuerzburg.de
[6] Scott Polar Research Institute, University of Cambridge, England - ear53@cam.ac.uk
[7] Austrian Institute of Technology, Center for Vision, Automation and Control, Austria - Jules.Salzinger@ait.ac.at
[8] Department of Geography, University of Innsbruck, Austria – (martin.rutzinger, andreas.mayr)@uibk.ac.at
* all authors contributed equally

Keywords: Peat Erosion, Geomorphology, Uncrewed Aerial Vehicle Laser Scanning, Airborne Laser Scanning, M3C2 Change Detection, Time Series Classification.

Abstract

Peatlands play an important role as local carbon sinks and climate archives in natural environments. In addition to degradation by human activities, peatlands can also be affected by geomorphological processes such as fluvial erosion. This study used a collection of multi-temporal 3D point clouds to investigate such a situation in a valley of the Central Alps (Austria), where a dynamically migrating river is eroding peat. To detect time periods and locations where strong erosion occurred and to quantify the local peat erosion rate over the years 2006 to 2024, 3D point clouds from airborne laser scanning (ALS), uncrewed aerial vehicle laser scanning (ULS), and uncrewed aerial vehicle photogrammetry (UPH) were used (i) in a pair-wise Multiscale Model-to-Model Cloud Comparison (M3C2) change detection and quantification and (ii) in a time-series clustering approach. In the most dynamic sections of the river bank, the mean rate of peat erosion over the eighteen-year period was -0.12 ± 0.03 m/year. Moreover, the relationship between peatland erosion and main channel migration is investigated based on a set of surface elevation transects and multi-temporal mapping of the main channels. Overall, these methods provided detailed insights into the dynamics and functioning of local geomorphological processes, such as lateral undercutting with subsequent toppling and sliding of the peat bank.

1. Introduction

Peatlands play an important role as carbon sinks (Amesbury et al., 2019) and constitute rich environmental archives (Gearey and Fyfe, 2016). Peat is partially decomposed organic matter and, as a proportion of dry mass, blanket peat is typically around 50% carbon (Dawson et al., 2004). Thus, mass loss from peatlands represents a significant carbon source. Most studies on peatland carbon budgets have concentrated on gas flux, with less attention given to carbon export by geomorphological processes, such as fluvial erosion (Li et al., 2018). During high discharge events, rivers can erode peat through undercutting and channel collapse (Härkönen et al., 2023). Furthermore, the likelihood of peatlands becoming a source as opposed to a sink for carbon in the future, is exacerbated by atmospheric warming (Gallego-Sala et al., 2018). With mountain areas being typically characterized by strong geomorphological dynamics and, at the same time particularly affected by contemporary climate warming (Pepin et al., 2022), the recent development and future prospects of high-altitude peatlands, including the effects of erosion, are of particular interest.

In addition to traditional methods such as erosion pins, bounded plots and sediment traps, erosion research has increasingly applied modern topographic surveying methods. Detailed topographic models from laser scanning or photogrammetry can be repeatedly applied to peatlands to improve the quantification of erosion (Passalacqua et al., 2015; Okyay et al., 2019; Li et al., 2018). Uncrewed aerial vehicle laser scanning (ULS) combines advantages of terrestrial laser scanning (TLS; high resolution and flexibility) with those of airborne laser scanning (ALS; larger areal productivity and view from above). Hence, repeat ULS surveys have been used as a particularly valuable tool for monitoring landslides and erosion in grasslands (Mayr et al., 2019a), or for deep-seated gravitational slope deformations (Zieher et al., 2019). To improve temporal coverage ULS data can be combined with ALS data that has been acquired with a wider application scope and for larger areas using topographic LiDAR sensors onboard crewed aircraft (Mayr et al., 2019a; Zieher et al., 2019).

In addition to digital elevation model (DEM) differencing, topographic distances computed directly from 3D point clouds are increasingly used for erosion change detection and analysis. This enables distance to be measured in any direction, avoids subsampling and interpolation during rasterization, and as a result, is more accurate in complex environments (Passalacqua et al., 2015). However, much existing research only analyses two or three epochs (i.e., point cloud acquisitions from different points in time), but with the growing availability of efficient sensing systems and, hence, opportunities for data collection, multi-temporal analyses is increasingly used. In many cases, the exploitation of time as the fourth dimension advances the geomorphological understanding of process dynamics and

This contribution has been peer-reviewed. The double-blind peer-review was conducted on the basis of the full paper.
https://doi.org/10.5194/isprs-annals-X-G-2025-937-2025 | © Author(s) 2025. CC BY 4.0 License.

drivers (Eitel et al., 2016). A pairwise comparison of changes between successive epochs of a multi-temporal point cloud collection can reveal detailed spatio-temporal patterns of processes such as erosion, transport, and deposition (Mayr et al., 2019b). Furthermore, time series analysis, such as time series clustering (Kuschnerus et al., 2021) and spatial region growing based on time series similarity (Anders et al., 2021), use temporal information to recognise topographic change patterns in space and time.

In this paper, we aim to investigate the dynamics and patterns of fluvial erosion of a peatland in the Central Alps (Austria) on an interannual to decadal time scale. This is achieved by analysing a series of ULS and ALS point clouds through multi-temporal 3D distance calculation, channel mapping, interpretation of elevation transects, and time series clustering.

2. Study Area and Data

2.1 Study Area

We investigate a section of the Rotmoos Valley close to the village of Obergurgl (Austria). The river Rotmoos Ache drains a catchment of approximately 10 km^2, of which approximately 4 km^2 was glaciated in 2010 (Koch and Erschbamer, 2010). At an elevation of approximately 2,260 m above sea level (a.s.l). the river forms a braided river system (Figure 1A), with dynamically migrating channels and gravel bars (Backes et al., 2020). Along its orographic right (northeastern) riverbank, a peatland area stretches for approximately 800 m (Figure 1B), with up to 2.65 m thick peat having formed since approximately 4000 BC (Bortenschlager, 2010). Field observations of the steep peat wall at the riverbank being eroded and of peat blocks being spread along the foot of the wall and downstream across the braided plain raise questions regarding the spatio-temporal patterns and rate of peat erosion. The following sections describe how we investigated these aspects using 4D point cloud analysis.

Figure 1. Overview of the Rotmoos Valley (A) and a close-up of the peat edge (B). Photographs taken on 25th September 2024.

2.2 Multi-Temporal Point Clouds

We used a total of six epochs of point clouds acquired between 2006 and 2024 at irregular intervals, with different sensor-platform systems (Tab. 1). In 2019, 2021, and 2022 data was collected by uncrewed aerial vehicle laser scanning (ULS) with a Riegl RiCopter system (RIEGL, 2024). This comprises a Riegl VUX-1LR laser scanner and an Applanix AP20 inertial measurement unit (IMU) with a differential global navigation satellite system (DGNSS) receiver (Applanix, 2024). The IMU/GNSS data was postprocessed with Applanix POSPac (Applanix, 2024), and for subsequent point cloud extraction, georeferencing and strip adjustment dedicated Riegl software packages (RIEGL, 2024) were used.

In 2024, imagery along with camera position data was acquired with a DJI M350 RTK UAV (DJI, 2024) and processed with a structure-from-motion and multi-view stereo workflow in Agisoft Metashape 2.0.0 (Agisoft, 2024). The resultant UAV photogrammetric point cloud (referred to as UPH point cloud in the following) was validated from 12 independent DGNSS surveyed checkpoints. The mean errors for easting, northing, and ellipsoidal height were calculated as 0.013 m, 0.015 m, and 0.052 m, respectively. The monitoring period was extended back to 2006 and 2017 by airborne laser scanning (ALS) point clouds (Tab. 1) provided by the federal government of Tirol (Land-Tirol, 2024).

3. Methods

A pipeline to process the multi-temporal point clouds efficiently is shown in Figure 2, consisting of co-registration of all point clouds, bi-temporal distance computation with the Multiscale Model-to-Model Cloud Comparison (M3C2) method (Lague et al., 2013) for change detection and quantification, and time-series analysis based on k-means clustering. Details of each process are described below.

3.1 Point Cloud Co-Registration

First, the point clouds were cropped to the area of interest. The UPH point cloud obtained in 2024, which had the highest point density, was subsampled to match the approximate density of the ULS point clouds (Tab. 1). A variant of the iterative closest point (ICP) algorithm that includes an automatic detection of stable areas (Yang and Schwieger, 2023), implemented in the py4dgeo Python library (py4dgeo Team, 2023), was employed to co-register all point clouds. Stable areas identified from preliminary M3C2 calculations were used for validation, i.e., estimation of registration errors. The 2022 ULS point cloud was used as the co-registration reference, and the corresponding errors are shown in Table 1.

3.2 Topographic Change Detection and Quantification

To detect and quantify the topographic change in the study area and to estimate the peat erosion rates, we used the py4dgeo implementation (py4dgeo Team, 2023) of the M3C2 algorithm (Lague et al., 2013). The M3C2 computes the local surface distances of core points between two point clouds along the locally estimated surface normals. Using all the points of the 2024 UPH point cloud as core points, i.e., reference epoch, we applied M3C2 to calculate surface distances between each epoch and the reference epoch 2024. The normal and projection radius was set to a diameter of 0.5 m. We manually identified

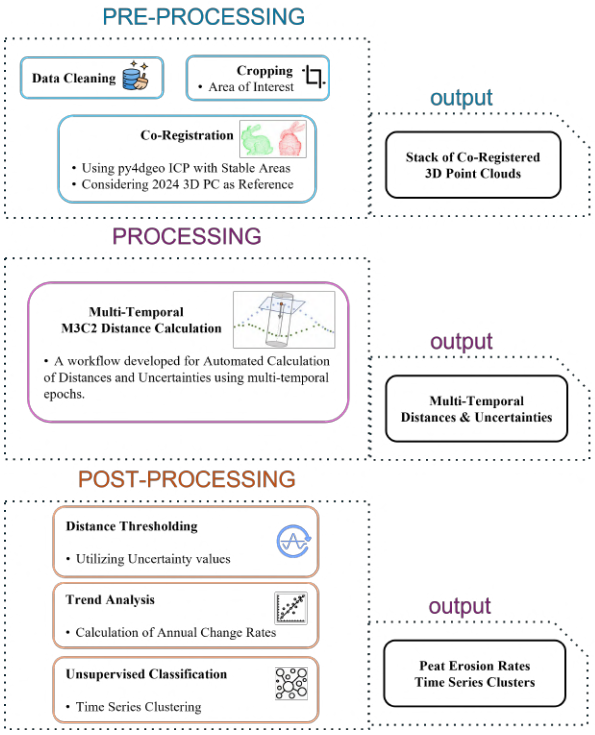

Figure 2. Schematic diagram of the processing pipeline.

four areas of 3 m in diameter, which we consider to be stable areas, and used the M3C2 distance between these stable areas (for each co-registered point cloud pair) as an estimate for the registration error (Tab. 1, column 4). Along with the local point density and a planarity estimate, these registration errors are used to calculate a spatially varying uncertainty estimate for the distances. This is referred to as the Level of Detection (LoD), i.e. the minimal detectable change at the 95% confidence interval (Lague et al., 2013). The resulting LoD for all scans is summarised in Table 1, column 5. Aiming to exclude 3D distances resulting from low point density, measurement noise, and co-registration errors, M3C2 distances are thresholded with the LoD at the same point. Hence, only change distances exceeding the LoD are considered significant changes and further analyzed.

3.3 Time series Clustering and Peat Detection

To differentiate spatiotemporal patterns of surface change, we performed a k-means clustering with the time series of surface distances between the six epochs of point clouds as proposed, for instance by Kuschnerus et al. (2021). Therefore, a spatiotemporal array of M3C2 distances at the core points was constructed, i.e., each timestamp had the same number of points representing surface changes. The number of clusters (i.e., k) was determined using the Elbow method for optimal internal clustering criteria. We chose the Sum of Squared Errors of samples to their closest cluster center to evaluate the clustering results (Syakur et al., 2018). From evaluating between 2 to 10 clusters, we chose k = 6, which shows the ”elbow point” between the number of clusters and inertia criteria. This k-means clustering is essentially an unsupervised classification of the point clouds, from which two clusters were identified corresponding spatially to the area of the eroding peat cliff observed in the field (Figure 5). For these clusters, we calculate the peat erosion rate between each epoch as the M3C2 distance divided by the difference in years.

3.4 Transects Analysis

To track the development of the braid plain and the riverbanks, including the peat, across the monitoring period, we generated a series of digital elevation models (DEMs) with 0.5 m cell size by aggregating the mean Z value for each cell using CloudCompare. Then, six elevation profiles (transects) across the braid plain and the riverbanks were extracted from the DEMs (Figure 3).

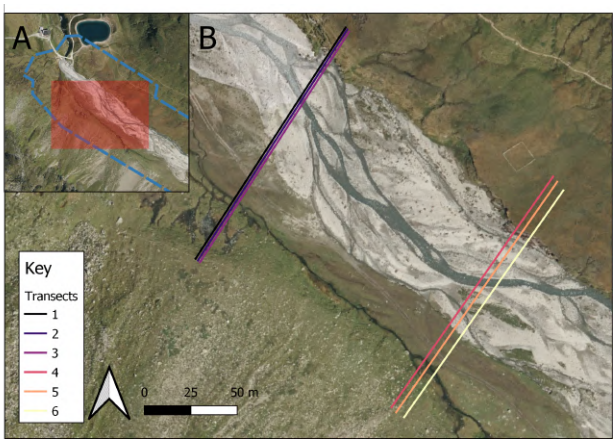

Figure 3. Transects for the geomorphological analysis.

4. Results

4.1 Co-registration and M3C2 Distance

The implemented pipeline (Figure 2) successfully processed the collection of multi-temporal point clouds, including co-registration, topographic change detection and quantification, and time-series clustering analysis. The 2006 airborne LiDAR point cloud has the lowest point density (3.18 ± 1.91 pts/m^2) and the lowest accuracy among the datasets, as expected. The mean registration error and LoD with this epoch are 0.08 m (2006/2022) and 0.17 m (2006/2024), respectively. For the 2017 ALS point cloud, the point density is 21.78 ± 7.88 pts/m^2 and the LOD is 0.06 ± 0.02 m. For the UAV LiDAR and UPH point clouds, acquired at much closer ranges (lower flying height) and with much higher point densities, the LoD is approximately in the range 0.04 m to 0.07 m (Tab.1).

Figure 4 visualizes the M3C2 distances for each epoch with respect to the 2024 UPH point cloud and these distances are summarized in Table 1. The darker red represents higher erosion of the peat areas. The focus on the peat areas at the northeast side of the riverbank reveals that the M3C2 distances had negative values within the observation period, indicating the long-term erosion process (Figure 4).

4.2 Time Series Clustering and Erosion Rate of the Peat Banks

Figure 5 shows the results of the time-series clustering. Generally, flatter terrain outside the braid plain and the gentle foot slopes remained stable in the monitoring period (cluster 3; colored dark green in Figure 5). Cluster 0 (colored light green) contains only small distances except for some stronger variation due to seasonal snow patches persisting mainly at the

This contribution has been peer-reviewed. The double-blind peer-review was conducted on the basis of the full paper.
https://doi.org/10.5194/isprs-annals-X-G-2025-937-2025 | © Author(s) 2025. CC BY 4.0 License.

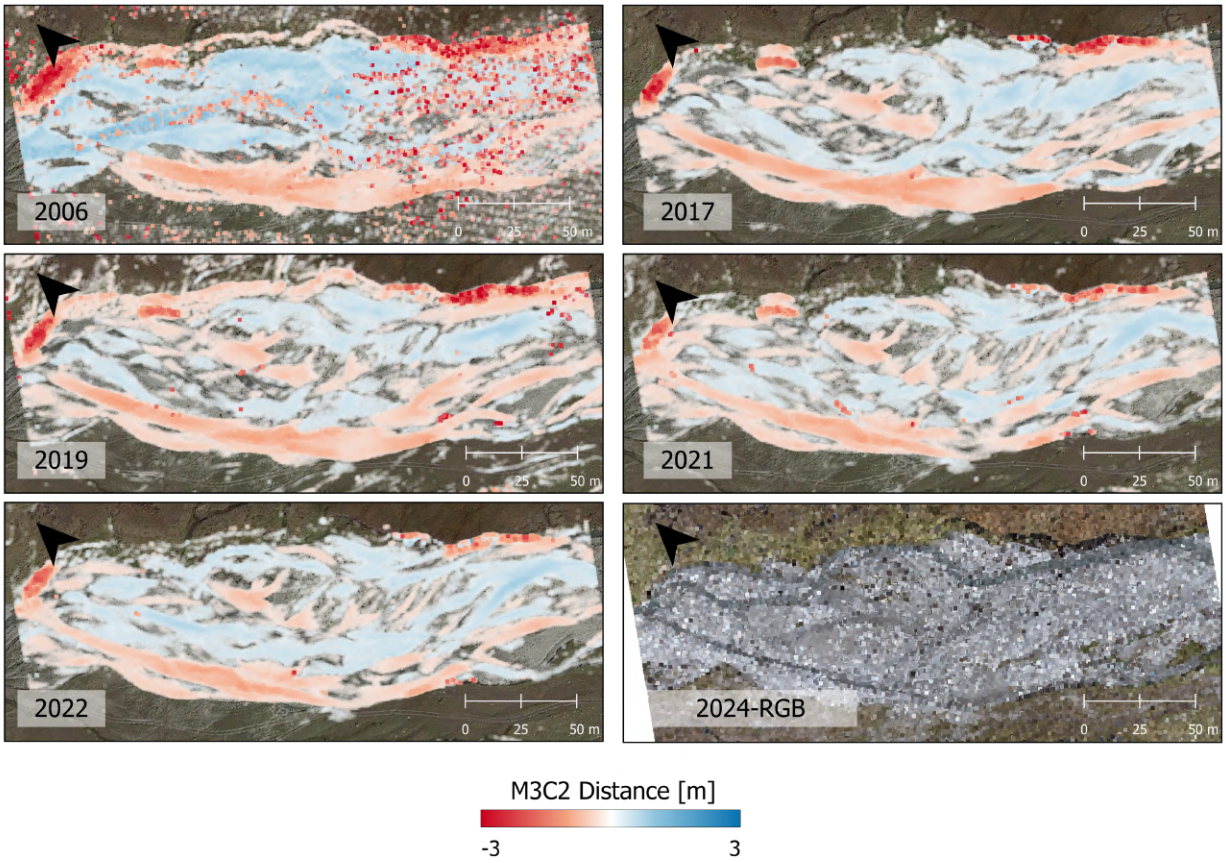

Figure 4. M3C2 distances calculated with respect to the 2024 UPH point cloud. The negative and positive values represent surface changes between each epoch and the reference epoch (2024 UPH). Erosion (negative values) and accumulation (positive values) are visualized in red and blue, respectively.

Year Acquisition	Mean point density ± std (pts/m^2)	Mean registration error (m)	M3C2 distance ± std (m)	Mean LoD ± std (m)
2006 ALS	3.18 ± 1.91	0.080	0.02 ± 0.03	0.17 ± 0.09
2017 ALS	21.78 ± 7.88	0.061	0.06 ± 0.02	0.06 ± 0.02
2019 ULS	382.76 ± 209.00	0.055	0.06 ± 0.03	0.07 ± 0.01
2021 ULS	255.62 ± 132.75	0.054	0.04 ± 0.02	0.04 ± 0.01
2022 ULS	259.94 ± 124.35	reference	0.00 ± 0.03	0.06 ± 0.01
2024 UPH	213.71 ± 46.79	0.057	reference	reference

Table 1. Summary of point cloud datasets and statistics of co-registration and M3C2 distances. The 2022 and 2024 point clouds were used as the reference dataset in the co-registration and M3C2 calculation processes, respectively.

foot slopes in the 2019 point cloud. Clusters 1 and 2 (brown and gray) are interpreted as fluvial sediment aggradation and erosion within the dynamically evolving braid plain. We found clusters 4 (blue) and 5 (red) representing erosion of the peat bank at the orographically right (i.e., northeastern) riverbank (Figure 5), corresponding to our field observations. Thus, we identify P_1, P_2 and P_3 are three areas where peat erosion occurs actively from 2006 to 2024.

The statistics of the change rate of peat areas (Figure 6) demonstrate two different erosion patterns: the erosion of cluster 4 is more linear and more spatially concentrated, while the erosion of cluster 5 has a linear decrease accompanied by stabilization after a period of sharp decrease between 2006 and 2017, while the spatial distribution is more dispersed around cluster 4. From this, we can see that the central area of the peat shows a steady erosion from year to year, while the surrounding areas may show irregular changes, such as abrupt changes potentially due to undercutting and subsequent collapse of the bank.

Based on the time series of surface distances along the local normal direction (i.e., orthogonal to the surface), we calculated the mean and the standard deviation of the change rate for each time step (Figure 6). For clusters 4 and 5, the mean erosion rate across all epochs is -0.12 ± 0.03 m/year from 2006 to 2024. As shown in Figure 7, erosion occurred for all epochs in clusters 4 and 5 besides time steps 2017-2019.

The spatial distribution of the accumulation subareas fits the erosion sites in earlier periods, pointing to a distinct mechanism of bank erosion processes. This is composed of lateral undercutting of the riverbank by the river, followed by a toppling (or sliding) of peat from the upper part of the steep bank. The peat may temporarily accumulate at the bottom (see Figure 1B) until it is evacuated by the river during high discharge.

4.3 Transects Analysis

As shown in Figure 3 and 5, Transects 1 to 3 and Transects 4 to 6 are located close to P_1 and P_2 identified by the time-series clustering, respectively. In addition to the mean erosion rate calculated for each cluster by clustering time-series analysis, the terrain profiles at these transects provide information on how dynamically the riverbanks and the braidplain are devel-

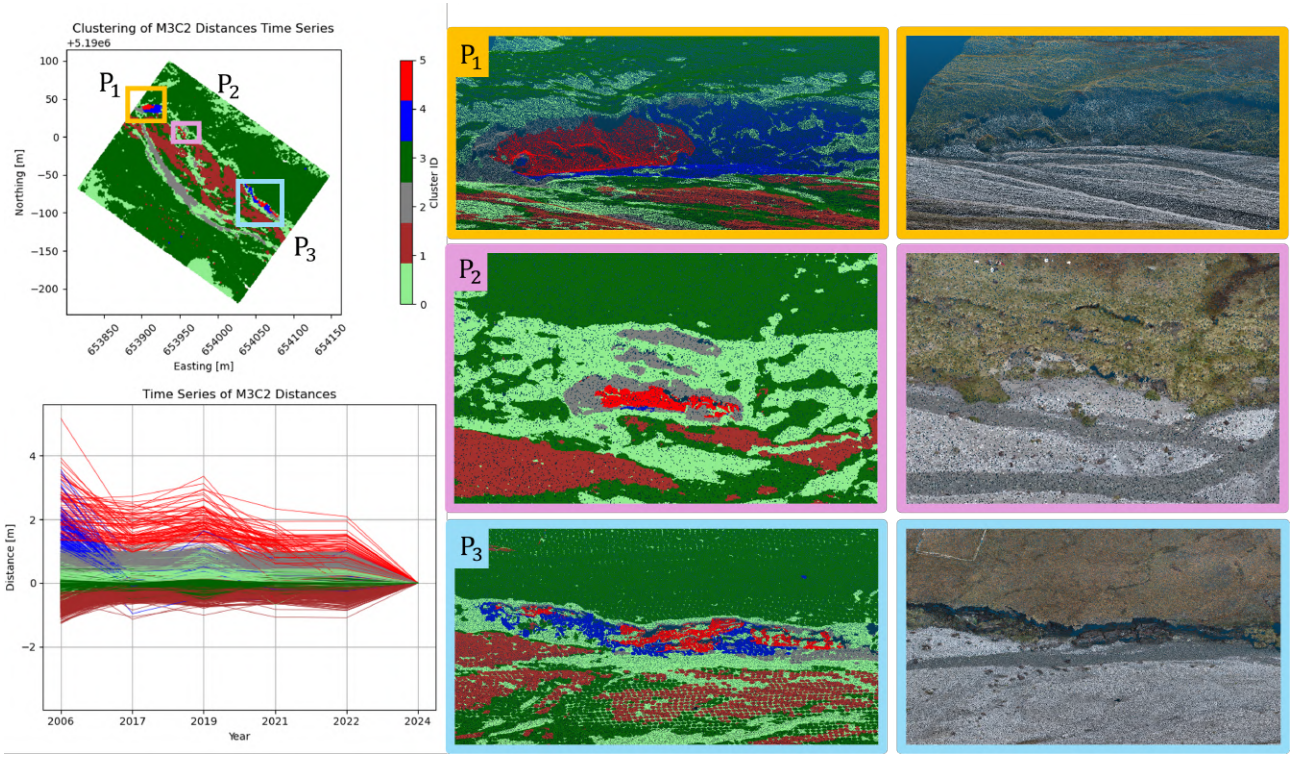

Figure 5. The cluster map of the M3C2 time series and time series colored by cluster IDs. Cluster 4 (blue) and cluster 5 (red), highlighted by colored boxes, fit the peat cliff spatially and demonstrate two different temporal patterns of erosion across 2006 - 2024.

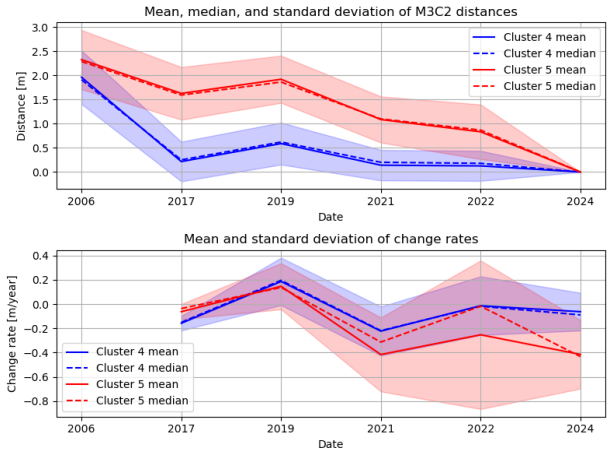

Figure 6. The measured significant distance (i.e., change) and annual change rates for clusters 4 and 5 (corresponding to the peat banks).

oping in different sections. Figure 4 shows that the orographically right (i.e., northeastern) riverbank has been subject to larger terrain changes ($>$ 3 m surface lowering) than the left one since 2006. Moreover, compared to Transect 1, the upstream riverbed (Transect 6) fluctuated more during the analytical period, especially the riverbed at the right bank. From Figrue 7, we observed that different rates of change can be found at various locations within the two transects. For Transect 1, lower parts of the peat wall (at an elevation of 2,307.30 m a.s.l.) exhibit the highest erosion rate of -1.10 m/year between 2021 and 2022, followed by a decreased rate (-0.31 m/year) during the next two years. In contrast, the surface remained stable at the upper part of the peat wall (2,308.50 m a.s.l.) in the same period. At Transect 6, the lower part of the peat wall (2,311.00 m a.s.l.) had the highest erosion activity from 2019 to 2021 with a rate of -1.95 m/year, followed by an erosion rate of -1.63 m/year in the last two years. The upper peat wall (2,312.80 m a.s.l.) was affected by similar erosion magnitudes, but the rate of change decreased to -0.33 m/year in both periods. Moreover, the lower peat wall in Transect 6 shows significant accumulation from

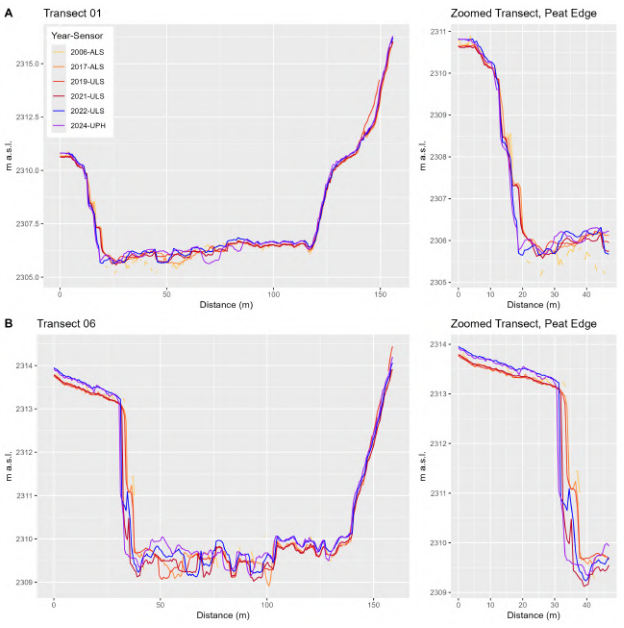

Figure 7. Elevation profiles in direction NE to SW along (A) Transect 1 and (B) Transect 6 between 2006 to 2024.

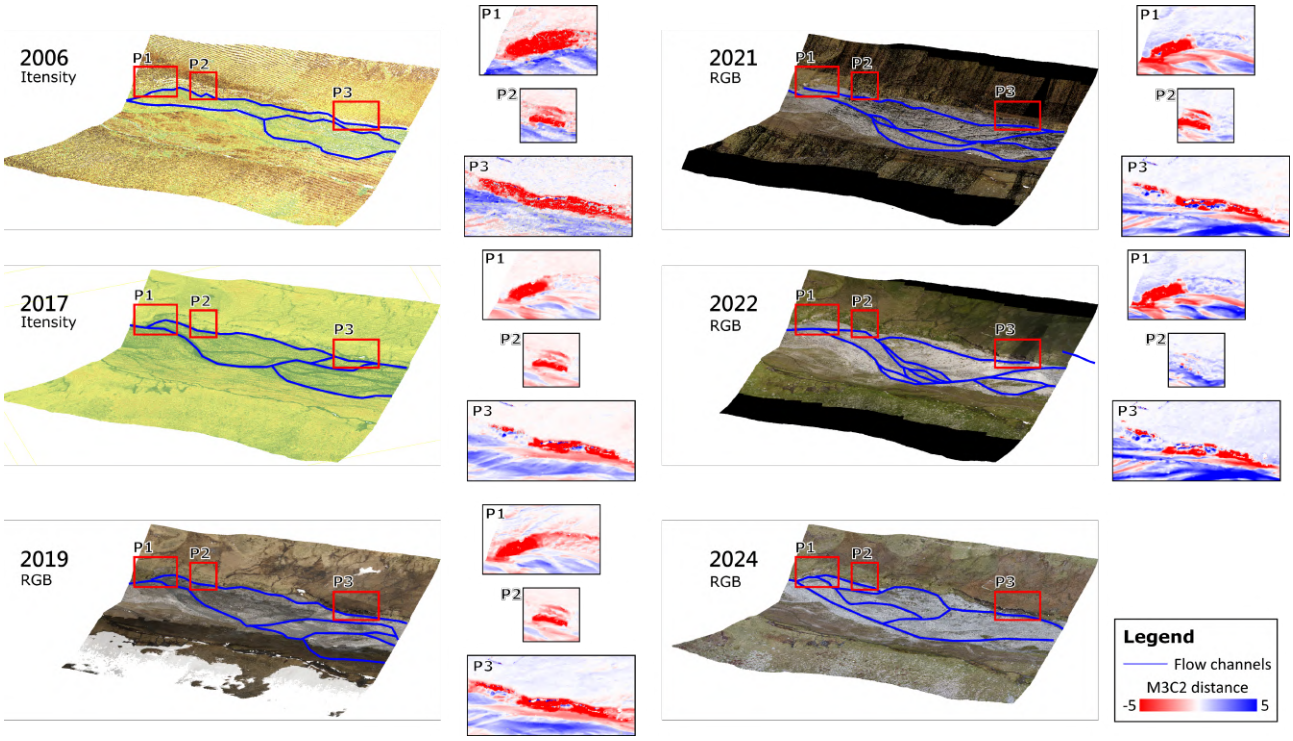

Figure 8. Main channel migration and peatland erosion from 2006 to 2024. Map subsets show close-up oblique views of the point cloud distances.

2021 to 2022, with an accumulation rate of 2.60 m/year (Figure 7). This observation fits the positive change rate revealed by the clustering time-series analysis (Figure 6).

5. Discussion

We first note the lower quality of the ALS point clouds, notably the one from 2006. Noise results in spurious negative distances in some parts of the area, as is visible in Figure 4. This is interpreted as less accurate strip adjustment within the earliest epoch and might (partly) be mitigated by filtering outlier points. Furthermore, the lower density of these point clouds and the lack of consistently stable areas in peat bogs and braided river systems present challenges for an automated co-registration and distance computation pipeline. Nonetheless, the obtained registration results and distance patterns otherwise confirm the good performance of the method by Yang and Schwieger (2023) for areas with unclear stable areas.

Furthermore, channel patterns over time were identified by visually interpreting the multi-temporal point clouds with either RGB color or laser return intensity values (2006 and 2017 ALS point clouds are not colourized). Due to the low reflectivity of water, the river channels can be well identified. As shown in Figure 8, most channels showed the typical morphodynamics of a braided river system and migrated to some extent throughout the monitoring period. Hence, we conclude that channel migration, together with peak discharge events, is a key factor controlling spatio-temporal dynamics of peat erosion in the Rotmoos Valley.

6. Conclusion

In the presented study, the acquisition and analysis of 4D point clouds enabled the detailed reconstruction and quantification of topographic change and, more specifically, impacts of fluvial processes on peatland in an Alpine valley bottom from 2006 to 2024. Using a combination of topographic point clouds from airborne laser scanning (ALS), and from uncrewed aerial vehicle laser scanning (ULS) and photogrammetry (UPH), respectively, made it possible to investigate peat erosion dynamics over 18 years. On the one hand, the first point cloud epoch (of 2006) brings relatively high uncertainties concerning change detection due to its lower density and accuracy. On the other hand, it extends the time series relatively far beyond the period of ULS availability, which is valuable for the analysis of geomorphic process dynamics.

For time steps of varying length, we quantified the magnitudes of 3D surface change and associated change rates. The development of peat erosion related to flow channel migration was interpreted with 2D topographic profiles and 3D M3C2 results over time. Moreover, our study illustrates how time series clustering on the point clouds can be a valuable unsupervised classification tool, as it identifies relevant spatial units for further interpretation and for quantitative analysis of, e.g., erosion rates. This reveals detailed spatio-temporal patterns of surface change and provides new insights into erosion dynamics. In the future, further progress could be made by continued monitoring at the site, ideally by transitioning towards higher-frequency (e.g., daily) observations using a permanent laser scanning system and linking these to discharge measurements.

Acknowledgements

This study was conducted within the Innsbruck Summer School of Alpine Research 2024 – Close Range Sensing Techniques in Alpine Terrain, (https://www.uibk.ac.at/en/geography/sensing-mountains/2024/). The ULS point clouds of 2019 – 2022 were acquired and pre-processed by the Remotely Piloted Aircraft

Team of the Department of Geography at the University of Innsbruck. ALS point clouds of 2006 and 2017 were provided by the Office of the Federal Government of Tirol, Division of Geoinformation (Land Tirol, https://data.tirol.gv.at). The authors would like to thank Prof. Katharina Anders and the whole thermal imagery calibration group for sharing resources and helping during fieldwork.

References

Agisoft, 2024. Agisoft Metashape: Professional Edition. https://www.agisoft.com/features/professional-edition/.

Amesbury, M. J., Gallego-Sala, A., Loisel, J., 2019. Peatlands as Prolific Carbon Sinks. *Nature Geoscience*, 12(11), 880–881.

Anders, K., Winiwarter, L., Mara, H., Lindenbergh, R., Vos, S. E., Höfle, B., 2021. Fully Automatic Spatiotemporal Segmentation of 3D LiDAR Time Series for the Extraction of Natural Surface Changes. *ISPRS Journal of Photogrammetry and Remote Sensing*, 173, 297–308.

Applanix, 2024. Trimble Applanix : POS Pac Products Family. https://www.applanix.com/products/pospac.htm.

Backes, D., Smigaj, M., Schimka, M., Zahs, V., Grznárová, A., Scaioni, M., 2020. RIVER MORPHOLOGY MONITORING OF A SMALL-SCALE ALPINE RIVERBED USING DRONE PHOTOGRAMMETRY AND LIDAR. *The International Archives of the Photogrammetry, Remote Sensing and Spatial Information Sciences*, XLIII-B2-2020, 1017–1024.

Bortenschlager, S., 2010. Vegetationsgeschichte im Bereich des Rotmoostales. *Glaziale und periglaziale Lebensräume im Raum Obergurgl*, 77–91.

Dawson, J. J., Billett, M. F., Hope, D., Palmer, S. M., Deacon, C. M., 2004. Sources and Sinks of Aquatic Carbon in a Peatland Stream Continuum. *Biogeochemistry*, 70(1), 71–92.

DJI, 2024. Matrice 350 RTK. https://enterprise.dji.com/de/photo.

Eitel, J. U. H., Höfle, B., Vierling, L. A., Abellán, A., Asner, G. P., Deems, J. S., Glennie, C. L., Joerg, P. C., LeWinter, A. L., Magney, T. S., Mandlburger, G., Morton, D. C., Müller, J., Vierling, K. T., 2016. Beyond 3-D: The New Spectrum of Lidar Applications for Earth and Ecological Sciences. *Remote Sensing of Environment*, 186, 372–392.

Gallego-Sala, A. V., Charman, D. J., Brewer, S., Page, S. E., Prentice, I. C., Friedlingstein, P., Moreton, S., Amesbury, M. J., Beilman, D. W., Björck, S., Blyakharchuk, T., Bochicchio, C., Booth, R. K., Bunbury, J., Camill, P., Carless, D., Chimner, R. A., Clifford, M., Cressey, E., Courtney-Mustaphi, C., De Vleeschouwer, F., de Jong, R., Fialkiewicz-Koziel, B., Finkelstein, S. A., Garneau, M., Githumbi, E., Hribjlan, J., Holmquist, J., Hughes, P. D. M., Jones, C., Jones, M. C., Karofeld, E., Klein, E. S., Kokfelt, U., Korhola, A., Lacourse, T., Le Roux, G., Lamentowicz, M., Large, D., Lavoie, M., Loisel, J., Mackay, H., MacDonald, G. M., Makila, M., Magnan, G., Marchant, R., Marcisz, K., Martínez Cortizas, A., Massa, C., Mathijssen, P., Mauquoy, D., Mighall, T., Mitchell, F. J. G., Moss, P., Nichols, J., Oksanen, P. O., Orme, L., Packalen, M. S., Robinson, S., Roland, T. P., Sanderson, N. K., Sannel, A. B. K., Silva-Sánchez, N., Steinberg, N., Swindles, G. T., Turner, T. E., Uglow, J., Väliranta, M., van Bellen, S., van der Linden, M., van Geel, B., Wang, G., Yu, Z., Zaragoza-Castells, J., Zhao, Y., 2018. Latitudinal Limits to the Predicted Increase of the Peatland Carbon Sink with Warming. *Nature Climate Change*, 8(10), 907–913.

Gearey, B., Fyfe, R., 2016. Peatlands as Knowledge Archives. *Peatland Restoration and Ecosystem Services: Science, Policy and Practice*, 95–114.

Härkönen, L. H., Lepistö, A., Sarkkola, S., Kortelainen, P., Räike, A., 2023. Reviewing peatland forestry: Implications and mitigation measures for freshwater ecosystem browning. *Forest Ecology and Management*, 531, 120776.

Koch, E.-M., Erschbamer, Brigitta, U., 2010. *Glaziale und periglaziale Lebensräume im Raum Obergurgl*. innsbruck university press.

Kuschnerus, M., Lindenbergh, R., Vos, S., 2021. Coastal Change Patterns from Time Series Clustering of Permanent Laser Scan Data. *Earth Surface Dynamics*, 9(1), 89–103.

Lague, D., Brodu, N., Leroux, J., 2013. Accurate 3D Comparison of Complex Topography with Terrestrial Laser Scanner: Application to the Rangitikei Canyon (N-Z). *ISPRS Journal of Photogrammetry and Remote Sensing*, 82, 10–26.

Land-Tirol, 2024. Land Tirol Open Government Data. https://www.tirol.gv.at/data/.

Li, C., Grayson, R., Holden, J., Li, P., 2018. Erosion in Peatlands: Recent Research Progress and Future Directions. *Earth-Science Reviews*, 185, 870–886.

Mayr, A., Bremer, M., Rutzinger, M., Geitner, C., 2019a. UNMANNED AERIAL VEHICLE LASER SCANNING FOR EROSION MONITORING IN ALPINE GRASSLAND. *ISPRS Annals of the Photogrammetry, Remote Sensing and Spatial Information Sciences*, IV-2-W5, 405–412.

Mayr, A., Rutzinger, M., Geitner, C., 2019b. Object-Based Point Cloud Analysis for Landslide and Erosion Monitoring. *Photogrammetric Engineering & Remote Sensing*, 85(6), 455–462.

Okyay, U., Telling, J., Glennie, C. L., Dietrich, W. E., 2019. Airborne Lidar Change Detection: An Overview of Earth Sciences Applications. *Earth-Science Reviews*, 198, 102929.

Passalacqua, P., Belmont, P., Staley, D. M., Simley, J. D., Arrowsmith, J. R., Bode, C. A., Crosby, C., DeLong, S. B., Glenn, N. F., Kelly, S. A., Lague, D., Sangireddy, H., Schaffrath, K., Tarboton, D. G., Wasklewicz, T., Wheaton, J. M., 2015. Analyzing High Resolution Topography for Advancing the Understanding of Mass and Energy Transfer through Landscapes: A Review. *Earth-Science Reviews*, 148, 174–193.

Pepin, N., Arnone, E., Gobiet, A., Haslinger, K., Kotlarski, S., Notarnicola, C., Palazzi, E., Seibert, P., Serafin, S., Schöner, W. et al., 2022. Climate changes and their elevational patterns in the mountains of the world. *Reviews of Geophysics*, 60(1), e2020RG000730.

py4dgeo Team, 2023. Py4dgeo: Library for change analysis in 4D point clouds. https://github.com/3dgeo-heidelberg/py4dgeo.

RIEGL, 2024. RIEGL - RIEGL Laser Measurement Systems. http://www.riegl.com/.

Syakur, M. A., Khotimah, B. K., Rochman, E. M. S., Satoto, B. D., 2018. Integration K-Means Clustering Method and Elbow Method For Identification of The Best Customer Profile Cluster. *IOP Conference Series: Materials Science and Engineering*, 336(1), 012017.

Yang, Y., Schwieger, V., 2023. Supervoxel-Based Targetless Registration and Identification of Stable Areas for Deformed Point Clouds. *Journal of Applied Geodesy*, 17(2), 161–170.

Zieher, T., Bremer, M., Rutzinger, M., Pfeiffer, J., Fritzmann, P., Wichmann, V., 2019. ASSESSMENT OF LANDSLIDE-INDUCED DISPLACEMENT AND DEFORMATION OF ABOVE-GROUND OBJECTS USING UAV-BORNE AND AIRBORNE LASER SCANNING DATA. *ISPRS Annals of the Photogrammetry, Remote Sensing and Spatial Information Sciences*, IV-2-W5, 461–467.